

LThA3.pdf

# Geiger-mode Avalanche Photodiode Focal Plane Arrays for 3D LIDAR Imaging

M. A. Itzler, M. Entwistle, M. Owens, K. Patel, X. Jiang, K. Slomkowski, and S. Rangwala

*Princeton Lightwave Inc., 2555 US Route 130 South, Cranbury, NJ 08512 USA  
mitzler@princetonlightwave.com*

**Abstract:** We describe FPAs based on planar-geometry Geiger-mode avalanche photodiodes designed for single-photon 3D LIDAR imaging systems. We compare new 32x128x50 $\mu\text{m}$  format FPAs with 32x32x100 $\mu\text{m}$  FPAs for dark count rate, crosstalk performance, and overall pixel yield.

**OCIS codes:** (040.1345) Avalanche photodiodes; (040.5570) Quantum detectors; (110.6880) Three-dimensional image acquisition; (280.3640) Lidar

## 1. Introduction

Relative to conventional two-dimensional (2D) imagers, new three-dimensional (3D) imaging technologies provide greatly enhanced capabilities for object detection and identification. The most effective approach for 3D image capture is the use of LIDAR techniques for high-resolution range measurements within the scene of interest [1]. Arrays of detectors capable of independent time-of-flight range measurements enable highly efficient collection of 3D images relative to legacy approaches involving the scanning of discrete detectors.

In this paper, we present results obtained from 3D imaging focal plane arrays (FPAs) employing planar-geometry InGaAsP/InP Geiger-mode avalanche photodiodes (GmAPDs) with high-efficiency single photon sensitivity at 1.06  $\mu\text{m}$ . We report the first results obtained for new 32 x 128 format FPAs with 50  $\mu\text{m}$  pitch and compare these results to those obtained for 32 x 32 format FPAs with 100  $\mu\text{m}$  pitch. We show excellent pixel-level performance—including 100% pixel operability—for both formats, and the array-level distribution of dark count rate (DCR) is found to be similar for both types of arrays. The optical crosstalk due to photon emission induced by pixel-level avalanche detection events is also found to be comparable for both formats, with worst-case nearest-neighbor pixels exhibiting < 1% crosstalk for photon detection efficiencies as high as 40%.

## 2. GmAPD focal plane array (FPA) design

The GmAPD FPA module is comprised of a number of critical sub-components, including a photodiode array (PDA) based on GmAPD pixels; a CMOS readout integrated circuit (ROIC) for pixel-level electrical interfacing and FPA-level control; a GaP microlens array (MLA) to ensure high fill factor; and various packaging sub-components to define electrical, mechanical, and optical interfaces to the overall hermetically sealed module. Details pertaining to this module design have been reported elsewhere [2,3]. To enable turnkey operation of the module, we have also designed FPGA-based electronics that control full camera-level operation.

To create FPAs with single-photon sensitivity at every pixel, we have employed a planar-geometry diffused-junction GmAPD discrete device design [4] in an array format. A quaternary InGaAsP absorber is optimized for detection of 1.06  $\mu\text{m}$  photons. (We have also achieved similar results for longer wavelength 1.55  $\mu\text{m}$  GmAPD FPAs using InGaAs absorbers [3].) The GmAPD array is flip-chip bonded to the CMOS ROIC, which controls all functions of the FPA, including biasing of the GmAPD pixels during user-selectable range gates from 10 ns to 10  $\mu\text{s}$  and high-speed readout enabling very high frame rates (up to 186 kHz with 2  $\mu\text{s}$  range gates for the 32 x 32 FPA). Space-efficient in-pixel pseudorandom counters [1] provide 13 bit time-stamp data encoding photon arrival times. Pixel-level ROIC circuitry was designed to ensure compatibility with both 100  $\mu\text{m}$  and 50  $\mu\text{m}$  pitch formats.

Following the hybridization of the PDA to the ROIC, we align and attach a GaP microlens array (MLA) to the back surface of the PDA. The MLAs provide an effective fill factor of ~75% in coupling to the 34  $\mu\text{m}$  diameter active regions of the 32 x 32 x 100  $\mu\text{m}$  pitch FPAs and to the 18  $\mu\text{m}$  diameter active region of the 32 x 128 x 50  $\mu\text{m}$  pitch FPAs. The resulting chip stack of ROIC+PDA+MLA is attached to a ceramic interposer which provides electrical signal routing, and a two-stage thermoelectric cooler stabilizes temperature 55  $^{\circ}\text{C}$  below ambient.

## 3. Comparison of FPA dark count rate for 32x32 and 32x128 sensors

The most important characteristic of the GmAPD FPA is the fundamental tradeoff between DCR and PDE. Higher PDE can be achieved by operating at higher excess bias voltage, but only at the expense of increased DCR. The

LThA3.pdf

map in Figure 1 (at left) illustrates the DCR performance for all 1024 pixels of the 32 x 32 array. These data demonstrate perfect yield, with 100% pixel operability (i.e., all pixels within target specifications for DCR and PDE performance). The DCR distribution for the entire array (Figure 1, at right) has an average of 13.6 kHz and a standard deviation of 4.2 kHz. Additionally, *all* 1024 pixels in the array exhibit a DCR < 20 kHz for the specified operation conditions. The corresponding PDE distribution, reported elsewhere [2], shows a value of 39% ± 6.3%, which includes all optical losses such as the microlens array effective fill factor.

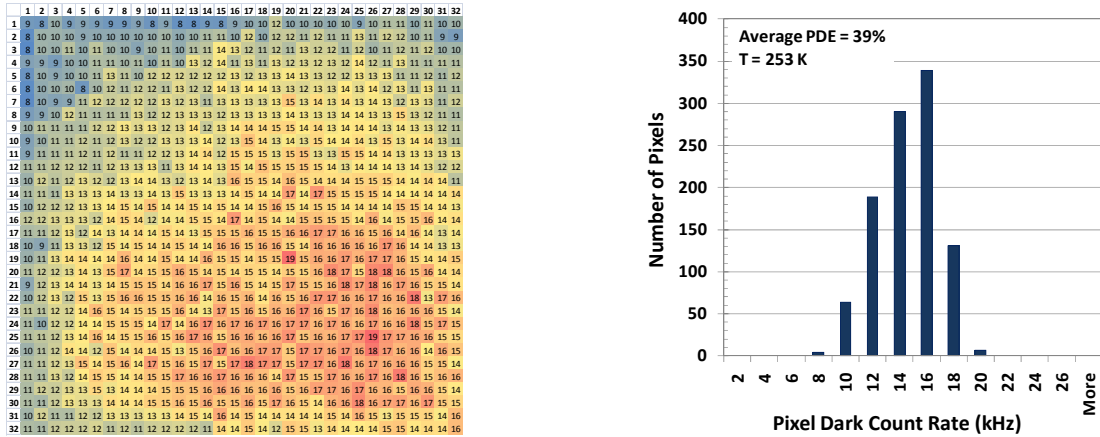


Fig. 1. Dark count rate (DCR) data in kHz obtained for a 32 x 32 FPA designed for 1064 nm photon detection showing 100% pixel operability. DCR mapping (left) and a DCR histogram (right) show that *all* 1024 pixels exhibit DCR < 20 kHz at 253 K and average photon detection efficiency (PDE) of 39% (which includes microlens array coupling).

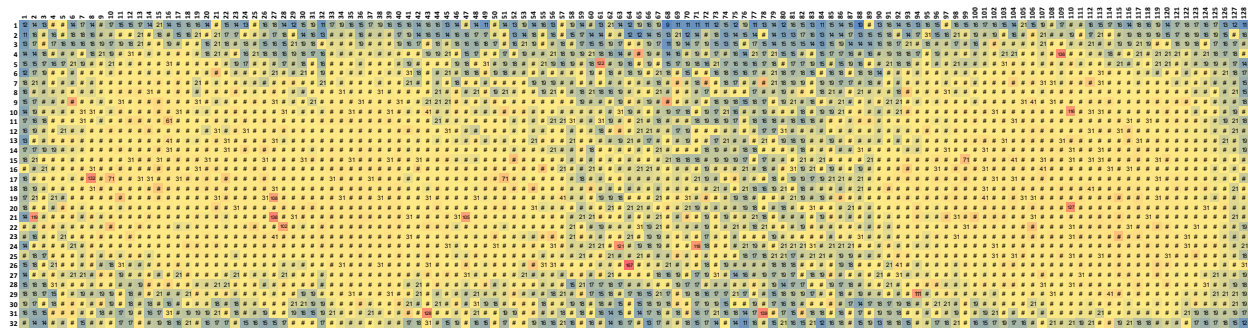


Fig. 2. Dark count rate (DCR) map for a 32x128 FPA designed for 1064 nm photon detection showing 100% pixel operability at pixel-level PDE ~ 35% and 253 K. Approximately 20 pixels have elevated DCR (between 100 and 175 kHz) but are still operable.

In Figure 2, we present a map of DCR performance for all 4096 pixels of a 32x128 format FPA. As in the case of the 32 x 32 FPA, we have achieved 100% pixel operability, although about 0.5% of the pixels have somewhat elevated DCR between 100 and 175 kHz. The DCR distribution for the entire FPA, presented on the left side of Figure 3, has a mean value of 26 kHz and a standard deviation of 10 kHz. DCR values were obtained at an excess bias voltage of 2.5 V, which provided a corresponding “detector-level” PDE (i.e., without MLA) of about 35%. On this particular module, FPA-level PDE data was degraded by misalignment of the MLA.

On a second FPA assembled without a microlens array, we characterized the array-level PDE by considering just that portion of the broad-area optical illumination which fell within the active area of the detector—i.e., this “per-pixel” PDE value does not include any fill factor effects. With these data, we obtain the DCR vs. PDE dependence shown on the right side of Figure 3 for 11 representative pixels across the array. This behavior is comparable to analogous data taken on 32 x 32 FPAs [2] after scaling for active area size and microlens fill factor effects, although these data for the new 32 x 128 FPAs exhibits a somewhat wider distribution, presumably due to the larger size of the array.

4. Comparison of FPA crosstalk behavior for 32x32 and 32x128 sensors

Optical crosstalk can occur in GmAPD arrays when an avalanche of electrical carriers in one pixel emits photons due to hot carrier luminescence (1 emitted photon for every ~10<sup>5</sup> to 10<sup>6</sup> avalanche carriers). The single photon sensitivity of neighboring pixels makes them susceptible to correlated counts triggered by these luminescence

LThA3.pdf

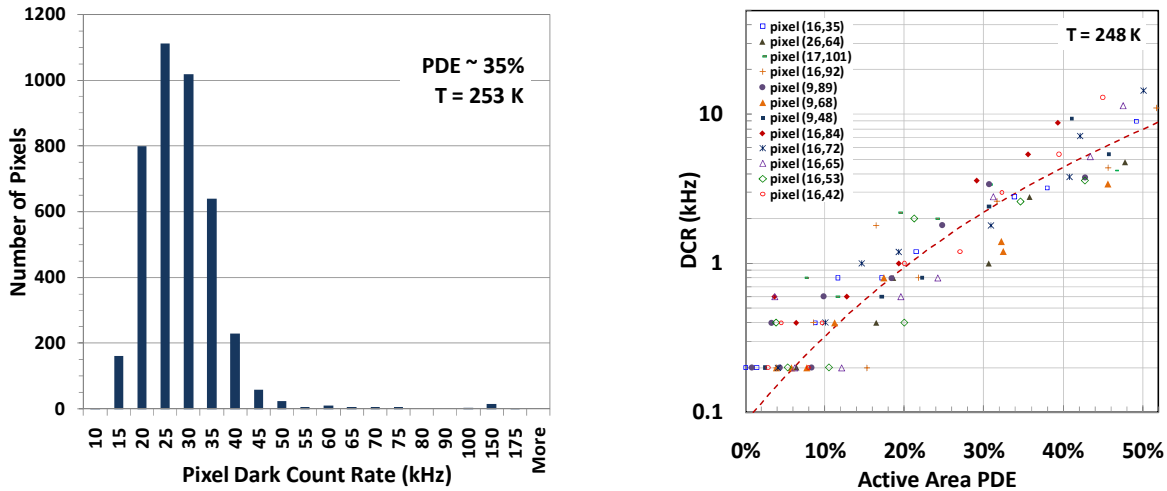


Fig. 3. Left: DCR histogram for the 32 x 128 FPA DCR map presented in Fig. 2. Right: DCR vs. PDE for 11 typical pixels of a second 32x128 FPA where pixel-level PDE data was obtained without microlenses.

photons. To reduce the line-of-sight coupling between nearest-neighbor pixels, we have etched isolation trenches along the pixel boundaries. Crosstalk is characterized by triggering an avalanche in one particular pixel using focused single photon illumination and then looking for correlated avalanches in neighboring detectors. We find that correlated cross-talk events occur within a few ns of the initial avalanche and tend to decay over a distance of  $\sim 500 \mu\text{m}$ . In Figure 4, we should the probability of cross-talk events as a function of the distance of neighboring pixels from the initial avalanche. For the 32 x 32 (left) and 32 x 128 (right) formats, we find a similar “fingerprint” pattern that is reproducible and depends on the specific optical path connecting the avalanching pixel to a particular neighboring pixel. Near- and next-nearest neighbors have larger crosstalk due to direct line-of-sight optical paths, whereas crosstalk at further neighbors involves photon reflections from the back surface of the PDA chip. However, even worst-case near neighbors have cross talk probabilities of  $< 1\%$  for PDE  $\sim 40\%$ .

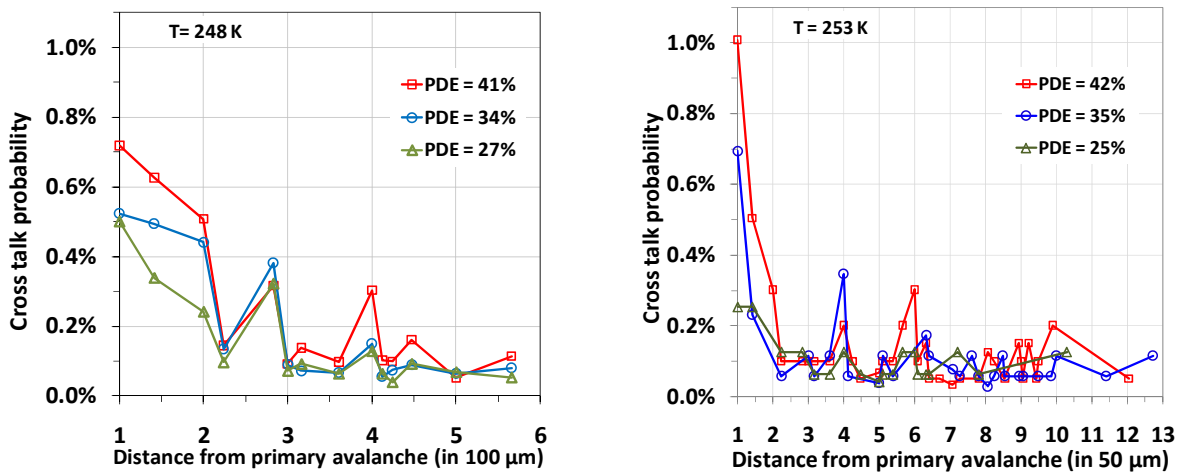


Fig. 4. Measured crosstalk probability per pixel as a function of distance from the pixel exhibiting initial avalanche (in units of center-to-center pixel pitch). Data from 32x32 FPAs with 100  $\mu\text{m}$  pitch (left) and from 32x128 FPAs with 50  $\mu\text{m}$  pitch (right) are similar.

[1] M. A. Albota, B. F. Aull, D. G. Fouche, *et al.*, “Three-dimensional imaging laser radars with Geiger-mode avalanche photodiode arrays,” *MIT Lincoln Laboratory Journal* **13**, no. 2, p. 351 – 370 (2002).  
 [2] M. A. Itzler, M. Entwistle, M. Owens, K. Patel, X. Jiang, K. Slomkowski, S. Rangwala, P. F. Zalud, T. Senko, J. Tower, J. Ferraro, “Geiger-mode avalanche photodiode focal plane arrays for three-dimensional imaging LADAR,” *Proceedings of the SPIE* **7808**, 78080C (2010).  
 [3] M. A. Itzler, M. Entwistle, M. Owens, K. Patel, X. Jiang, K. Slomkowski, S. Rangwala, P. F. Zalud, T. Senko, J. Tower, J. Ferraro, “Design and performance of single photon APD focal plane arrays for 3-D LADAR imaging,” *Proceedings of the SPIE* **7780**, 77801M (2010).  
 [4] M. A. Itzler, X. Jiang, M. Entwistle, K. Slomkowski, M. Owens, A. Tosi, F. Acerbi, F. Zappa, and S. Cova, “Advances in InGaAsP-based avalanche diode single photon detectors,” *J. Modern Optics* **58**, Nos. 3–4, 174 – 200 (2011).